Translation-Invariant Contourlet Transform and Its Application to Image Denoising

Ramin Eslami, *Member, IEEE*, and Hayder Radha, *Senior Member, IEEE*

***Abstract*—Most subsampled filter banks lack the feature of translation invariance, which is an important characteristic in denoising applications. In this paper, we study and develop new methods to convert a general multichannel, multidimensional filter bank to a corresponding *translation-invariant* (TI) framework. In particular, we propose a *generalized algorithme à trous*, which is an extension of the *algorithme à trous* introduced for 1-D wavelet transforms. Using the proposed algorithm, as well as incorporating modified versions of directional filter banks, we construct the *TI contourlet transform* (TICT). To reduce the high redundancy and complexity of the TICT, we also introduce *semi-translation-invariant contourlet transform* (STICT). Then, we employ an adapted bivariate shrinkage scheme to the STICT to achieve an efficient image denoising approach. Our experimental results demonstrate the benefits and potential of the proposed denoising approach. Complexity analysis and efficient realization of the proposed TI schemes are also presented.**

***Index Terms*—Algorithme à trous, bivariate shrinkage, filter banks, image denoising, translation invariance (TI), translation-invariant contourlet transform (TICT).**

NOMENCLATURE

APS	Additions per input sample.
BLS-GSM	Bayes least-squares estimate using Gaussian scale mixtures.
BS	Bivariate shrinkage.
CT	Contourlet transform.
DFB	Directional filter bank.
DTCWT	Dual-tree complex wavelet transform.
FB	Filter bank.
GAT	Generalized *algorithme à trous*.
HDFB	Horizontal DFB.
HT	Hard thresholding.
LP	Laplacian pyramid.
MPS	Multiplications per input sample.
QFB	Quincunx filter bank.
STICT	Semi-TI contourlet transform.
TI	Translation-invariant.
TICT	TI contourlet transform.
TIDFB	TI directional filter bank.
TILP	TI Laplacian pyramid.
TIWT	TI wavelet transform.
VDFB	Vertical DFB.
WT	Wavelet transform.

Manuscript received June 3, 2005; revised March 29, 2006. The associate editor coordinating the review of this manuscript and approving it for publication was Dr. Theirry Blu.

R. Eslami was with the Department of Electrical and Computer Engineering, Michigan State University, East Lansing, MI 48824 USA. He is now is with the Department of Electrical and Computer Engineering, McMaster University, Hamilton, ON L8S 4K1, Canada (e-mail: reslami@ieee.org).

H. Radha is with the Department of Electrical and Computer Engineering, Michigan State University, East Lansing, MI 48824 USA (e-mail: radha@egr.msu.edu).

Digital Object Identifier 10.1109/TIP.2006.881992

I. INTRODUCTION

DURING the past decade, wavelets have proven their capability in many signal and image processing applications, such as compression and denoising [22]. Owing to the good nonlinear approximation property of wavelets for piecewise smooth signals, they have been very effective in generating efficient representation of 1-D waveforms. In the case of natural images in which piecewise regions are separated by smooth curves (or edges), however, one can still observe that there are self-similarities among the wavelet subbands. This implies that one is able to further process wavelet coefficients of an image in order to achieve more decorrelation. It is well known that wavelets are properly structured to treat point-wise singularities; hence, they are appropriate in representing piecewise smooth 1-D signals. In contrast, natural images contain singularities in the form of edges which need a more efficient transform than the *wavelet transform* (WT).

A. Background

An important factor of an effective image transform is directionality. Having this feature, a transform would be, in general, capable of handling singularities in 2-D signals effectively. Many directional transforms have been introduced in recent years. Continuous (directional) wavelets [1], complex wavelets [21], steerable pyramids [34], and brushlets [24] are some examples in the literature. The wavelet X-ray transform [38] and ridgelet transform [6] apply wavelets to the radon transform of an image in such a way that one could effectively represent arbitrarily oriented lines in an image. To make the ridgelet transform applicable to a natural image, the authors in [5] constructed curvelets using three steps: subband decompositions of the image, partitioning the subbands into blocks in such a way to satisfy the anisotropic scaling law, and then applying the ridgelet transform to the resulting blocks.

Using a similar idea of combining subband decomposition with a directional transform, Do and Vetterli introduced the *contourlet transform* (CT) [11]–[13]. In the CT, a *Laplacian pyramid* (LP) [4] serves as the first stage and *directional filter banks* (DFBs) [2] as the second stage. The LP is a redundant transform with a redundancy ratio of up to 4/3; thus, since the DFB is critically sampled, the redundancy factor of the CT is up to 4/3. Both the LP and the DFB involve subsampling in

their implementations and similar to the wavelet transform they are shift variant. It follows that the CT is also a shift-variant transform. An important advantage of translation invariance is that the performance of denoising applications is significantly improved when a *translation-invariant* (TI) scheme of a subsampled transform is employed. This advantage of TI schemes is achieved due to the elimination of the pseudo-Gibbs phenomenon artifacts resulting from thresholding the transform coefficients [8]. Translation-invariant (sometimes called *stationary* or *undecimated*) wavelets have been introduced in several studies [3], [8], [23], [25], [27]. TI denoising can be realized through the cycle-spinning algorithm [8], [18]. Cycle-spinning, clearly, is not an efficient way to perform TI denoising. Indeed, since wavelets are partially TI, by using an appropriate algorithm such as "*algorithme à trous*" [19], [33], the TI wavelet coefficients can be derived with low complexity, where only $N \log_2 N$ wavelet coefficients are needed to obtain the TI wavelets of a signal of size N, when using $L = \log_2 N$ levels.

B. Contributions of the Paper

In this paper, we propose methods for developing a TI scheme from a general multidimensional and multichannel subsampled *filter bank* (FB). In particular, we extend the *algorithme à trous* [19] introduced for 1-D wavelets to a "*generalized algorithme à trous*" (GAT), which is applicable to a general multidimensional subsampled (uniform or nonuniform) FB. We prove that the TI version of a subsampled FB obtained through the GAT provides a tight frame if the original subsampled FB has a tight frame. Using the proposed GAT along with employing modified versions of the DFB, we introduce the *TI contourlet transform* (TICT). Despite the utility of the proposed TICT for image denoising [16], its high redundancy in conjunction with its high complexity make this scheme less attractive for image processing applications. As a consequence, we propose *semi-TICT* (STICT). We also provide efficient realizations for the proposed TICT and STICT schemes. Subsequently, we propose a new image denoising scheme where we employ the STICT alongside the powerful bivariate shrinkage function [32] and show its capability when compared with some other leading denoising schemes.

C. Overview of the Paper

The outline of the paper is as follows. In Section II, we study and develop a TI scheme of a subsampled FB. Then, we propose a TI scheme of the CT in Section III. Section IV presents a new image denoising scheme based on the STICT along with the simulation results, and finally, our main conclusions are given in Section V.

II. Developing a TI Scheme for a Subsampled Filter Bank

In this section, we develop a TI version of a general multichannel and multidimensional FB. Translation invariance can be achieved through several ways. For instance, for a 1-D wavelet transform scheme with periodic extension, by appropriately shifting the signal at each level, we obtain different sets of transform coefficients, which altogether form a TI wavelet transform [16].

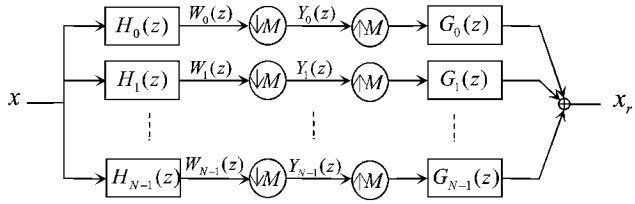

Fig. 1. Single-level multichannel filter bank.

Consider a perfect reconstruction d-dimensional N-channel FB as illustrated in Fig. 1. We denote M as a $d \times d$ sampling matrix. Note that if $N = d_M$, where $d_M = |\det(M)|$, the FB is critically sampled and if $N > d_M$, it is oversampled. We denote the outputs of the analysis filters before downsampling as $w_i[n]$, for $0 \le i < N$, where $n = (n_1, \ldots, n_d)^T \in \mathbb{Z}^d$. Hence, we have $y_i[n] = w_i[Mn]$. Below, we state a generalized procedure for obtaining all possible shifts of a multidimensional and multichannel FB.

Remark 1: If one computes all possible shifts of $w_i[n]$ (see Fig. 1) by[1] $k_c \in \mathcal{N}(M)$, $(0 \le c \le d_M - 1)$ that is, $\{w_i[n + k_c]\}_{0 \le c \le d_M - 1}$, where $d_M = |\det(M)|$, and $\mathcal{N}(M)$ is the set of integer vectors of the form Mt, $t \in [0, 1)^d$, then the output of the analysis section is translation invariant. It is clear that for a multilevel FB that one can apply the above method at each level for as many inputs as that level has.

In the next remark, we give an example that illustrates the fact that the existence of subsampling operations in a FB is not sufficient for shift variance of the FB. In what follows, we define $z^m \triangleq z_1^{m_1} \cdots z_d^{m_d}$, where $z = (z_1, \ldots, z_d)^T$ and $m = (m_1, \ldots, m_d)^T \in \mathbb{Z}^d$, and define $z^M \triangleq (z^{m_{c1}}, \ldots, z^{m_{cd}})^T$ where M is a $d \times d$ matrix with m_{ci} as its i th column. We also adopt the notation $z^{M^l} \triangleq z^{(M^l)}$ for an integer $l \in \mathbb{Z}$.

Remark 2: According to Remark 1, if in a critically sampled FB, without loss of generality, we have $w_i[n] = w_0[n + k_i]$ $(0 \le i \le d_M - 1)$ (suppose that $k_0 = \mathbf{0}$), the FB will be TI. In this case, the analysis and synthesis filters satisfy $H_i(z) = z^{k_i} H_0(z)$ and $G_i(z) = z^{-k_i} G_0(z)$, and $\{y_i[n]\}_{0 \le i \le d_M - 1}$ represent the polyphase components of $w_0[n]$. Consequently, the filter bank boils down to a simple nonsubsampled system with analysis filter $H_0(z)$ and synthesis filter $G_0(z)$, where $G_0(z) = 1/H_0(z)$ to ensure perfect reconstruction.

Using the procedure mentioned in Remark 1 to obtain a TI signal decomposition is appropriate in some applications such as adaptive coding, where we need to find a "best" shift based on a cost function. As a result, the method of finding a best tree as proposed in [7] is easily extendable to the multidimensional FB case with an arbitrary sampling matrix M. If however, we need the TI representation in some other applications (such as denoising) in which we require all the TI coefficients at the same time, we can use other approaches where we do not need to shift the coefficients. In what follows, we further discuss this aspect of the TI design.

[1]Note that, in general, this shift could be $k_c + mM$ where $m \in \mathbb{Z}^d$ is an arbitrary integer vector.

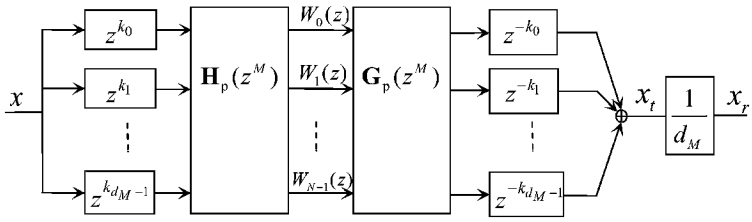

Fig. 2. Nonsubsampled (or TI) multichannel filter bank scheme in the polyphase domain.

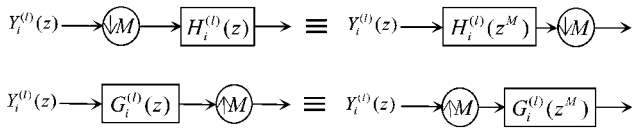

Fig. 3. Effects of subsampling on the filters of a filter bank should be considered when developing a TI scheme.

Remark 3: In a single-level multidimensional perfect reconstruction FB (see Fig. 1), omitting the sampling operations leads to a new TI output, x_t, which is a scaled version of x_r, i.e., $x_t = ax_r$, where $a = 1/d_M$ (see Fig. 2). Furthermore, the redundancy of the resulting TI filter bank equals N.

According to Remark 3, one can simply omit the subsampling operations at a single-level FB scheme to obtain a TI realization of the FB. For a multilevel FB, however, we cannot merely do so at every level to construct the corresponding TI scheme. In the nonsubsampled version of the FB, one has to change the analysis filters of level(s) $l > 1$ such that they operate the same way as if there is subsampling. In the next proposition, we show how one can construct new filters when one omits the subsampling operations in a multilevel FB, in order to achieve translation invariance.

Proposition 1 (Generalized Algorithme à Trous): Assume that we have an L-level octave-band multichannel FB with analysis and synthesis filters at level l as $H_i^{(l)}(z)$ and $G_i^{(l)}(z)$ $(0 \leq i \leq N, 1 \leq l \leq L)$, respectively, and a general d-dimensional sampling matrix M. If one omits the subsampling operations in the FB to obtain the TI scheme, the new analysis and synthesis filters at a level l $(1 \leq l \leq L)$ are $H_i^{(l)}(z) = H_i(z^{M^{l-1}})$ and $G_i^{(l)}(z) = G_i(z^{M^{l-1}})$, respectively.

Proof: We prove this proposition through induction. For the first level $(l = 1)$, as stated in Remark 3, the filters remain unchanged. Now, suppose we have the TI filters of $H_i^{(l)}(z) = H_i(z^{M^{l-1}})$ and $G_i^{(l)}(z) = G_i(z^{M^{l-1}})$ for a level l. Assume that the output of the analysis part at this level is $Y_i^{(l)}(z)$, $(0 \leq i < N)$. Now, at the next level, $l+1$, we apply a FB using the previous level filters, which are $H_i^{(l)}(z)$ and $G_i^{(l)}(z)$. Since in the original FB, each analysis (synthesis) filter presumes a downsampled (upsampled) version of the output of the last level, as depicted in Fig. 3, the equivalent filters are obtained using the noble identities: $H_i^{(l+1)}(z) = H_i^{(l)}(z^M)$ and $G_i^{(l+1)}(z) = G_i^{(l)}(z^M)$. Hence, $H_i^{(l+1)}(z) = H_i(z^{(M^{l-1})M}) = H_i(z^{M^l})$, and $G_i^{(l+1)}(z) = G_i(z^{(M^{l-1})M}) = G_i(z^{M^l})$. Note that according to Remark 3, one has to include a scaling factor equal to $1/d_M$ after each synthesis bank. □

The following corollary generalizes Proposition 1 when the sampling matrices are not the same.

Corollary 1: Suppose that M_l, $(1 \leq l \leq L)$ is the (d-dimensional) sampling matrix for the level l in the FB mentioned in Proposition 1. Then, the equivalent analysis and synthesis filters for the nonsubsampled FB for levels $l \leq 2$ (*they remain unchanged for the first level*) are $H_i^{(l)}(z) = H_i\left(z^{\left(\prod_{j=1}^{l-1} M_j\right)}\right)$, and $G_i^{(l)}(z) = G_i\left(z^{\left(\prod_{j=1}^{l-1} M_j\right)}\right)$, respectively. To ensure perfect reconstruction, a scaling factor equal to $1/d_{M_l}$ is required after each synthesis bank having the sampling matrix M_l.

In Proposition 1 and Corollary 1, we have extended the well-known *algorithme à trous* proposed in [19] for the wavelet transform to a *generalized algorithme à trous*, which is applicable to a general multidimensional multichannel FB system.

In Section III, we develop a TI scheme of the contourlet transform using the algorithms mentioned in this section.

III. Translation-Invariant Contourlet Transform

The contourlet transform is composed of two stages: a LP [4], [14] and DFB [2], [26]. The LP decomposes an image into a number of radial subbands plus an approximation image. Then, a DFB is applied to each resulting detail subband where a maximum number of directions are used at the finest subband, and this number of directional levels is decreased at every other radial detail subband to achieve the anisotropic scaling law of width$\propto$length^2 [5], [12]. Since the contourlet transform is realized using two stages of subsampled FBs, to create a TICT, we need to develop TI schemes for both stages as explained below.

A. Translation-Invariant Pyramids

A new reconstruction scheme was proposed for the LP that is based on the frame reconstruction, leading to more robustness against noise [14]. Fig. 4 shows the LP decomposition as well as its new reconstruction schemes. We let the sampling matrix, $\mathtt{M}$, be equal to diag(2,2) for images[2] where $\mathrm{diag}(a_1, a_2, \ldots, a_N)$ is defined as a diagonal $N \times N$ matrix having $(a_1, a_2, \ldots, a_N)$ as its diagonal elements. Here, H and G are the 2-D low-pass filter pair. Note that if one removes the subsampling operations from this LP framework, the resulting nonsubsampled FB will fail to be perfect reconstruction.

Do and Vetterli [14] proposed the LP in the polyphase domain [36], [37] in the form of an oversampled FB. In this form one can better observe the structure of the pyramids, and besides, it is a more suitable framework for developing the TI version of the

[2]While it is easily extendable to the multidimensional case, we present the 2-D LP, proper for image applications.

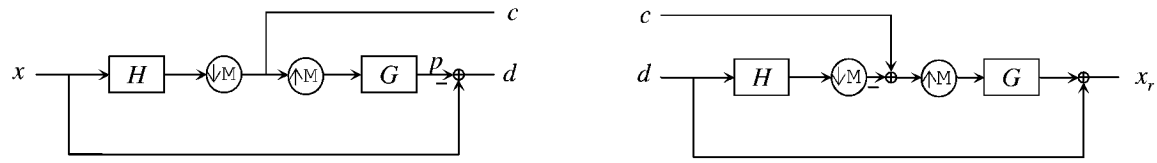

Fig. 4. Laplacian pyramid. (Left) The signal x is decomposed into a detail signal d and approximation c. (Right) The reconstruction scheme.

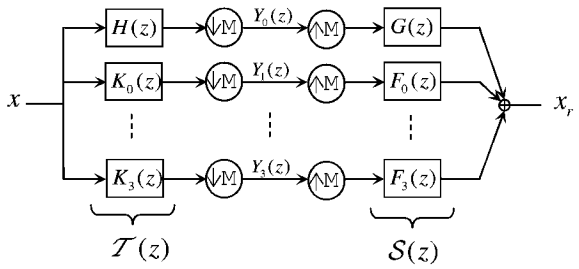

Fig. 5. Single-level 2-D LP in the form of an oversampled filter bank.

LP. Defining the vector of the polyphase components of a 2-D signal x in the z-domain as $X_{\mathcal{P}}(z) = (X_0(z), \ldots, X_3(z))^T$, and the filters h and g as the row and column vectors $H_{\mathcal{P}}(z) = (H_0(z), \ldots, H_3(z))$ and $G_{\mathcal{P}}(z) = (G_0(z), \ldots, G_3(z))^T$, one can write the input-output relationship of the LP as (see Fig. 5)

$$\mathcal{T}(z) = \begin{pmatrix} H(z) \\ z^{k_0} - G_0(z^{\mathtt{M}})H(z) \\ \vdots \\ z^{k_3} - G_3(z^{\mathtt{M}})H(z) \end{pmatrix} = \begin{pmatrix} H(z) \\ K_0(z) \\ \vdots \\ K_3(z) \end{pmatrix}. \quad (1)$$

Therefore, we have $Y(z) = \mathtt{D}_{\mathtt{M}}\{\mathcal{T}(z)X(z)\}$, where $\mathtt{D}_{\mathtt{M}}\{\cdot\}$ denotes the downsample operator using matrix $\mathtt{M}$. If the filters $h[n]$ and $g[n]$ are biorthogonal with respect to the sampling matrix $\mathtt{M}$, the inverse transform of the LP in the polyphase domain is found in the equation shown at the bottom of the page, and if $\mathtt{U}_{\mathtt{M}}\{\cdot\}$ denotes the upsample operator with respect to the matrix $\mathtt{M}$, we have (see Fig. 5)

$$X_r(z) = \mathcal{S}(z)\mathtt{U}_{\mathtt{M}}\{Y(z)\}.$$

Fig. 5 shows a single-level LP in the form of an oversampled FB. To construct a multilevel LP, one can simply iterate the single-level LP on the low-pass channel. Using the *generalized algorithme à trous* developed in Section II, the multilevel TI scheme of the LP is constructed by suppressing all subsampling operations and modifying the filters at a level l: $\mathcal{T}^{(l)}(z) = \begin{pmatrix} H(z^{\mathtt{M}^{l-1}}) & K_0(z^{\mathtt{M}^{l-1}}) & \cdots & K_3(z^{\mathtt{M}^{l-1}}) \end{pmatrix}^T$, and $\mathcal{S}^{(l)}(z) = \begin{pmatrix} G(z^{\mathtt{M}^{l-1}}) & F_0(z^{\mathtt{M}^{l-1}}) & \cdots & F_3(z^{\mathtt{M}^{l-1}}) \end{pmatrix}$, where $z^{\mathtt{M}^{l-1}} = (z_1^{2^{l-1}}, z_2^{2^{l-1}})$. This implies that we upsample the corresponding filters in both row and column directions with 2^{l-1}. Note also that we should scale the signal after each synthesis bank by 1/4. In the TILP scheme, since there are four detail channels at each level, the redundancy factor of this scheme is $4L + 1$, when an L-level system is employed. Below, we provide a brief discussion about the characteristics of the LP filters (Fig. 5).

As mentioned before, the LP is perfect reconstruction when the filter pair h and g are biorthogonal. Now we examine the condition in the case of the TILP.

Proposition 2: Upon omitting the subsampling operations in a single-level oversampled LP, if the filters h and g are biorthogonal then perfect reconstruction is guaranteed.

Proof: The proof is straightforward noting that

$$S(z)T(z) = 4 + G(z)H(z)\left(H_p(z^M)G_p(z^M) - 1\right).$$

Therefore, if $H_p(z^M)G_p(z^M) = 1$, we have perfect reconstruction. This condition is equivalent to $H_p(z)G_p(z) = 1$, which implies that the filters h and g are biorthogonal. The constant 4 indicates the need for a scaling factor. □

Consequently, removing subsampling operations from the LP does not eliminate the restriction of biorthogonality of filters h and g in the TILP frameworks. Now we take a closer look at the high-pass filters of the TILP.

Proposition 3: Let $H^{(1d)}(z)$ be a 1-D linear phase low-pass filter having multiple zeros at $z = -1$ as

$$H^{(1d)}(z) = (1+z)^{N_1}(1+z^{-1})^{N_1}R(z) \quad (2)$$

where $R(z) = R(z^{-1})$. Then, if $H_0^{(1d)}(z)$ and $H_1^{(1d)}(z)$ are polyphase components of $H^{(1d)}(z)$, $H_1^{(1d)}(z^2)$ has zeros at $z = \pm j$ or $w = \pm\pi/2$. In addition, $H_0^{(1d)}(z^2)$ and $H_1^{(1d)}(z^2)$ cannot have a zero at $z = -1$.

Proof: We can write $H_0^{(1d)}(z^2) = \mathrm{Even}\{H^{(1d)}(z)\}$ and $H_1^{(1d)}(z^2) = z^{-1}\,\mathrm{Odd}\{H^{(1d)}(z)\}$. Therefore, $H_1^{(1d)}(z^2)|_{z=\pm j} = \mp j2^{N_1-1}(R(j) - R(-j)) = 0$ and for the second part since $H^{(1d)}(z)$ is a low-pass filter, we have $H^{(1d)}(1) \neq 0$ and consequently, regarding (2) its even and odd parts are not zero at $z = -1$. □

$$\begin{aligned} \mathcal{S}(z) &= \begin{pmatrix} G(z) & z^{-k_0} - G(z)H_0(z^M) & \ldots & z^{-k_3} - G(z)H_3(z^M) \end{pmatrix} \\ &= \begin{pmatrix} G(z) & F_0(z) & \ldots & F_3(z) \end{pmatrix}, \end{aligned}$$

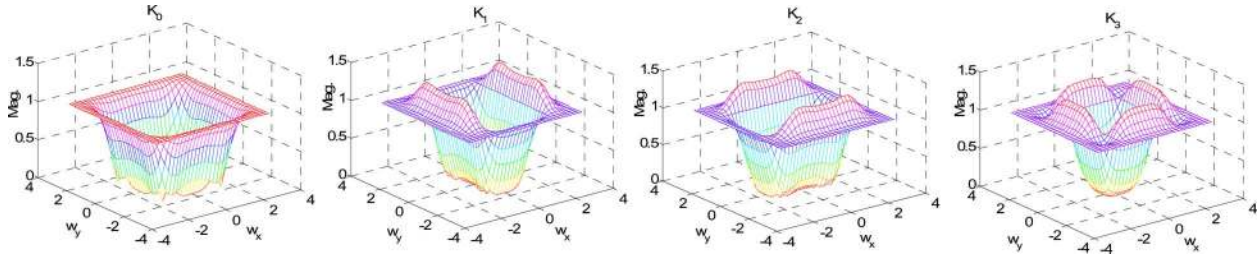

Fig. 6. Frequency responses of the high-pass analysis filters in the 2-D oversampled LP (Fig. 5). (Color version available online at http://ieeexplore.ieee.org.)

As a matter of fact, $H_1^{(1d)}(z^2)$ is also a low-pass filter with about half of the cutoff frequency of $H^{(1d)}(z)$. Note that the filters $G_i(z^{\mathrm{M}})H(z)$, $(0 \le i \le 3)$ in (1) are separable and obtained from 1-D filters $G_0^{(1d)}(z)H^{(1d)}(z)$ and $G_1^{(1d)}(z)H^{(1d)}(z)$, where they have zeros at $w = \pi$ and the latter has also zeros at $w = \pm\pi/2$. It turns out that the high-pass analysis LP filters $K_i(z)$, $(0 \le i \le 3)$—and, similarly, the synthesis filters $F_i(z)$—have passbands with different cutoff frequencies as illustrated in Fig. 6.

Note that, when we remove the subsampling operations in a FB, we encounter fewer restrictions in the filter design of such FBs. For instance, to ensure perfect reconstruction in a TI pyramid having five channels, the filters have to just fulfill the following condition:

$$H(z)G(z) + \sum_{i=0}^{3} K_i(z)F_i(z) = 1.$$

However, there is no standard method for designing 2-D filters having more than two channels with arbitrary passband regions. Moreover, the McClellan transformation, which is normally used in 2-D filter design, seems to be disadvantageous in designing 2-D multichannel FB. As a result, we resort to biorthogonal filters in the TILP similar to the LP. Next, a frame analysis is provided for a single-level TILP.

For redundant transforms, frames [9], [10] are efficient tools for analysis. A frame is defined as follows.

Definition: Let the sequence $\{\theta_j\}_{j\in\Gamma}$ and signal x, be in the Hilbert space $\mathcal{H}$; then $\{\theta_j\}_{j\in\Gamma}$ is a frame if there exist two constants $A > 0$, and $B < \infty$, such that, $A\|x\|^2 \le \sum_{j\in\Gamma} |\langle x, \theta_j\rangle|^2 \le B\|x\|^2$. We call A and B, the *frame bounds*. A frame is known as a *tight frame* when $A = B$. In a tight frame, the signal is reconstructed through $x = A^{-1}\sum_{j\in\Gamma}\langle x, \theta_j\rangle\,\theta_j$.

It is important to note that when a scheme can be expressed by a frame, it represents a stable framework, where the existence of an inverse transform is guaranteed. This is especially important for the schemes that are redundant. Since the LP is an oversampled FB, it could be better analyzed using frame theory. In the next proposition we prove that the TI realization of a single-level subsampled FB having a tight frame, is also a tight frame.

Proposition 4: Consider a single-level multidimensional FB (see Fig. 1) having a tight frame with frame bounds equal to one. Then, the corresponding TI FB provides a tight frame with frame bounds $A = B = d_M$.

Proof: From Remark 1, a technique to obtain a TI set of outputs is to shift the analysis filters by k_c, $(0 \le c \le d_M - 1)$. We also shift the synthesis filters, correspondingly. Hence, for each shift, we have a distinct set of kernel functions. Furthermore, each set provides a tight frame as we show it below. Assume the kernel functions of the original FB are $\{\theta_j\}_{j\in\mathbb{Z}^d}$; thus, the tight frame condition implies that $\sum_{j\in\mathbb{Z}^d} |\langle x, \theta_j\rangle|^2 = \|x\|^2$. Note that a shift in $\{\theta_j\}_{j\in\mathbb{Z}^d}$ corresponds to the same shift in x. As a result, the shifted version of the kernel functions is a distinct tight frame with frame bounds equal to one. Now suppose we denote the analysis kernel functions for a shift of k_c, by $\{\theta_j^c\}_{j\in\mathbb{Z}^d}$, where $0 \le c \le d_M - 1$. Let us denote $\{\varphi_j\} = \{\theta_j^c\}$, $(0 \le c \le d_M - 1$, and $j \in \mathbb{Z}^d)$, as the kernel functions of the TI FB. Then, we have

$$\sum_{j\in\mathbb{Z}^d} |\langle x, \varphi_j\rangle|^2 = \sum_{c=0}^{d_M-1} \sum_{j\in\mathbb{Z}^d} |\langle x, \theta_j^c\rangle|^2 = d_M\|x\|^2.$$

Therefore, the TI FB provides a tight frame with frame bounds $A = B = d_M$. □

As a result, if a subsampled FB provides a stable framework, the corresponding TI scheme also represents a stable realization.

Corollary 2: If the subsampled FB in Proposition 4 has a tight frame with frame bounds equal to K, then the corresponding TI scheme provides a tight frame with frame bounds $A = B = d_M K$.

Corollary 3: Since it is proven that a LP with orthogonal filters provides a tight frame [14], the single-level 2-D TILP with orthogonal filters provides a tight frame with frame bounds equal to four.

B. Translation-Invariant DFB

The DFB is a major part of the contourlet transform. It is realized through iterated quincunx FBs, and some resampling operations that just rearrange coefficients. In an $\hat{l}$-level DFB, we decompose the frequency space to $2^{\hat{l}}$ wedge-shaped partitions [Fig. 7(a)]. Using the noble identities, one can transfer all sampling operation to the end (beginning) of the forward (inverse) transform of the DFB [26]. As a result, one obtains $2^{\hat{l}}$ analysis and $2^{\hat{l}}$ synthesis filters, $H_i^{(\hat{l})}$ and $G_i^{(\hat{l})}$, respectively, and the overall sampling matrices $S_i^{(\hat{l})}$ $(1 \le i \le 2^{\hat{l}})$, as given below [12], [26]:

$$S_i^{(\hat{l})} = \begin{cases} \mathrm{diag}(2^{\hat{l}-1}, 2), & \text{for } 1 \le i \le 2^{\hat{l}-1} \\ \mathrm{diag}(2, 2^{\hat{l}-1}), & \text{for } 2^{\hat{l}-1} < i \le 2^{\hat{l}}. \end{cases}$$

Since it is the equivalent iterated DFB system for $\hat{l}$ levels, to construct the TI scheme, it is sufficient to suppress the sub-

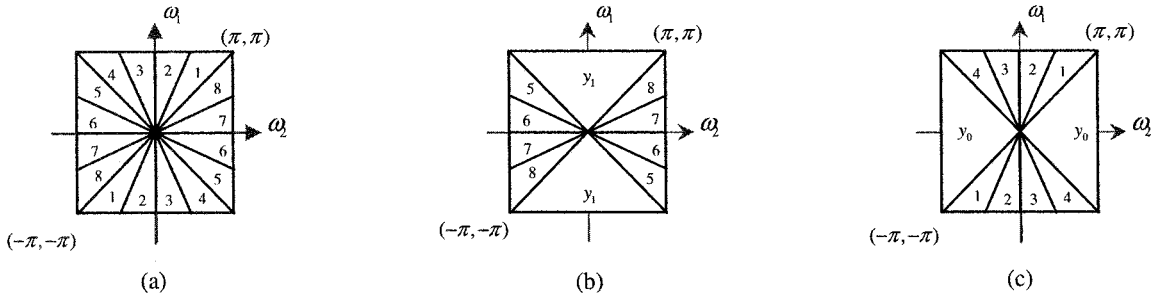

Fig. 7. (a) Frequency response of a DFB decomposed in three levels. (b) An example of the *vertical* directional filter banks with three levels. (c) An example of the *horizontal* directional filter banks with three levels.

sampling operations and multiply the reconstructed signal by a scaling factor, which is $1/\det(S_i^{(\hat{l})}) = 2^{\hat{l}}$ for both vertical and horizontal directions. Therefore, the redundancy factor of such a scheme is equal to the number of directions $2^{\hat{l}}$.

According to the passband regions of the TILP high-pass filters (see Fig. 6), in order to reduce complexity, for filters K_1 and K_2, it is appropriate to employ vertically and horizontally oriented DFBs [17], respectively (as we explain further in Section III-C). In *vertical DFB* (VDFB) and *horizontal DFB* (HDFB), we can achieve *mostly vertical* directions (directions between 45° and 135°) and *mostly horizontal* directions (directions between $-45°$ and $+45°$), as depicted in Fig. 7. In these two modified DFB schemes, we stop decomposing the signal horizontally or vertically after the first level of the DFB. Therefore, the overall sampling matrices for VDFB and HDFB will be

$$S_i^{V(\hat{l})} = \begin{cases} Q, & \text{for subband } y_1 \\ \operatorname{diag}(2, 2^{\hat{l}-1}), & \text{for } 2^{\hat{l}-1} < i \le 2^{\hat{l}}, \end{cases} \text{ and}$$

$$S_i^{H(\hat{l})} = \begin{cases} \operatorname{diag}(2^{\hat{l}-1}, 2), & \text{for } 1 \le i \le 2^{\hat{l}-1} \\ Q, & \text{for subband } y_0 \end{cases}$$

where Q is the quincunx sampling matrix. Note that we can change the shape of subbands y_0 and y_1 (see Fig. 7) in the spatial domain into a rectangle using a resampling matrix and shifting as explained in [17]. In the TI versions of the VDFB and HDFB, we should consider the new sampling matrices to obtain the proper scaling factors. The redundancy factor of the modified (either vertical or horizontal) TIDFB will be $2^{\hat{l}-1} + 1$.

Note that the construction provided for the (modified) TIDFB is not efficient in terms of complexity. We will present an efficient construction in Section III-D.

C. TI and Semi-TI Contourlet Transforms

We realize the *TI contourlet transform* (TICT) using the TILP and (modified) TIDFB. In fact, we employ a similar structure as the one used in the contourlet transform. However, when developing the TICT, since every level of the TILP has four high-pass subbands, we propose to apply the (modified) TIDFB to each one of these subbands. The form of passbands of high-pass filters in the TILP (Fig. 6) suggests to apply regular TIDFB to high-pass outputs of K_0 and K_3 and use TI VDFB and TI HDFB for outputs of K_1 and K_2, respectively. To preserve the anisotropic scaling law of width$\propto$length^2, we apply (modified) TIDFBs with a desired maximum number of directional levels to the four finest subbands of the TILP, where we are at level one, then as we decrease the radial resolution of the TILP at higher levels, we decrease the directional levels at every other TILP level.

Remark 4: Assume that a TILP has L levels and we apply $\hat{l}_i$-level $(1 \le i \le L)$ (modified) TIDFBs to the four detail subbands of level i of the TILP. Then the redundancy factor of the constructed TICT is $3L\sum_{i=1}^{L} 2^{\hat{l}_i} + 3$.

Improvement in denoising performance is an important reason justifying the construction of a TI version of a subband scheme. Since the redundancy of the (modified) TIDFB increases exponentially as the number of directional levels is raised, it makes the TICT highly redundant when comes along with the redundant transform of the TILP. Therefore, we propose another variety of the CT, which is less redundant and less complex. This new scheme is accomplished through applying the critically sampled (modified) DFBs to the TILP in much the same way that we employ the (modified) TIDFBs to realize the TICT. Hence, this contourlet realization is *not* TI, and, therefore, we refer to this approach as the STICT. The redundancy factor of this scheme is the same as that of the TILP, which is $4L + 1$.

Fig. 8 shows an example of the STICT of the *Boats* image using three TILP levels and (modified) DFBs with $\{\hat{l}_i\}_{1\le i\le 3} = \{3, 2, 2\}$ directional levels. Images at the top part of each level in this figure indicate the horizontal directions. We will denote the transform coefficients of the TICT and STICT by $\rho_{\mathtt{i},\mathtt{k}}^{(\mathtt{d})}(m)$ and $\eta_{\mathtt{i},\mathtt{k}}^{(\mathtt{d})}(m)$, respectively, where $\mathtt{i}$, $(1 \le \mathtt{i} \le L)$ indicates the pyramidal level, $\mathtt{k}$, $(1 \le \mathtt{k} \le 4)$ shows the pyramidal subband at each level, $\mathtt{d}$, $(1 \le \mathtt{d} \le 2^{\hat{l}_\mathtt{i}}$, for regular DFB) specifies the directional subband at each level, and m denotes the position in two dimensions. Likewise, we can also denote the CT coefficients by $\gamma_{\mathtt{i}}^{(\mathtt{d})}(m)$ with the same definition for $\mathtt{i}$, $\mathtt{d}$, and m.

Although the STICT is not TI, our preliminary image denoising results indicated the potential of this approach [16]. The main drawback of a shift-variant FB scheme to employ for denoising is due to the appearance of artifacts when one reconstructs the signal from not all of the transform coefficients. Here, we perform a simple experiment (similar to the one in [20]) to evaluate our proposed methods. First we obtain the transform of a synthetic image of a circle using the CT, TICT, and STICT (with $\{\hat{l}_i\}_{1\le i\le 3} = \{3, 2, 2\}$). Then, for each method, we reconstruct the image by keeping one directional subband at a

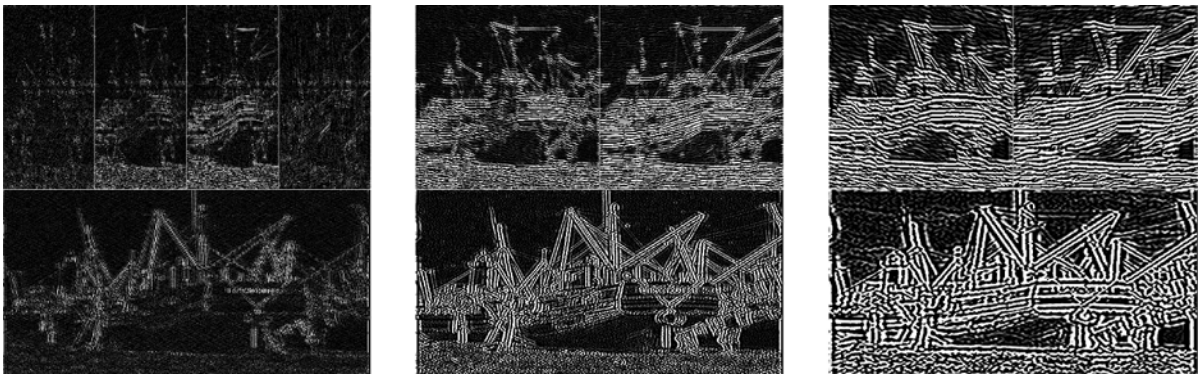

Fig. 8. Some of the STICT coefficients of the *Boats* image using $L = 3$ and $\{\hat{l}_i\}_{1<i<3} = \{3, 2, 2\}$ directional levels. The coefficients for only one TILP subband $(k = 3)$ are depicted. From left to right, the subbands $\eta^{(\mathtt{d})}_{1,3}$, $\eta^{(\mathtt{d})}_{2,3}$, and $\eta^{(\mathtt{d})}_{3,3}$ with all directions are shown. For better visualization, the transform coefficients have been clipped.

level $(L = \tilde{L})$ and its parents (ascendants) subbands in the other levels $(L < \tilde{L})$.

Fig. 9 shows some examples of the reconstructed images. It is clear that the images reconstructed using the CT show a lot of artifacts approving the unsuitability of this scheme for some image processing tasks such as image denoising. In contrast, the results of the TICT are almost artifact-free and have higher directional resolution. The STICT, interestingly, provides the results without noticeable difference to those of the TICT, which clarifies the importance of making the pyramidal subbands translation invariant. Hence, making the DFB stage translation invariant does not have significant impact in improving denoising results for the contourlet transform.

In Section III-D, we will provide fast realizations of the TILP and (modified) TIDFB, as well as the complexity analysis of the different proposed contourlet schemes.

D. Complexity Analysis and Efficient Realization

When employing the STICT and TICT, we encounter alternative FB schemes for which we propose and express efficient realizations along with their individual complexities; then, we specify the complexities of the above transforms. Note that we compute the complexities for the decomposition (analysis) stages while we have similar ones for the reconstruction (synthesis) banks.

1) LP: Since the sampling matrix $\mathtt{M}$ is separable, the 2-D filtering could be carried out in a separable mode using the 1-D filters $h^{(1d)}$ and $g^{(1d)}$ with lengths l_h and l_g, respectively. Therefore, from Fig. 4, we have $(l_h + l_g)/2$ *multiplications per input sample* (MPS) and $(l_h + l_g - 2)/2$ *additions per input sample* (APS) (note that the input to the filter G has $N^2/4$ nonzero samples for an input image of size $N \times N$). For a multilevel LP, the complexity is up to 4/3 the complexity of a single-level LP.

2) TILP: Considering the transfer function of a single-level TILP (1), although the filters K_i, $(0 \leq i \leq 3)$ are indeed nonseparable, we can do the filtering in a separable mode by computing the difference of the filtered input image (by first $H(z)$ and then $G_i^{\mathtt{M}}(z)$, which are both separable filters) from the input image shifted by k_i. Since $H(z)$ is a common filter in all the channels, we are just required to filter the input image

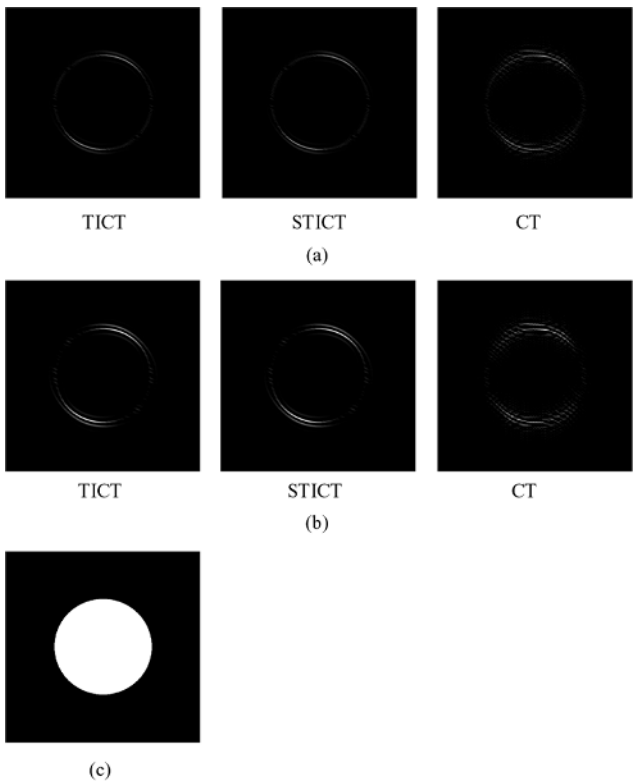

Fig. 9. (a) Reconstructed images using the subbands $\gamma^{(1)}_{\mathtt{i}}$, $\rho^{(1)}_{\mathtt{i},\mathtt{k}}$, and $\eta^{(1)}_{\mathtt{i},\mathtt{k}}$ for $1 \leq \mathtt{i} \leq 3$, and $1 \leq \mathtt{k} \leq 4$. (b) Images reconstructed using the subband(s) with indices $\mathtt{d} = 1$, $\mathtt{i} = 3$, and $1 \leq \mathtt{k} \leq 4$. (c) Original image.

by this filter once, which needs $2l_h$ MPS and $2l_h - 2$ APS. Now, without loss of generality, suppose that l_g is odd, then the polyphase components of $g^{(1d)}$ (denoted by $g_0^{(1d)}$ and $g_1^{(1d)}$) will have the lengths of $(l_g - 1)/2$ and $(l_g + 1)/2$. Meanwhile, the filters $G_i^{\mathtt{M}}(z)$, $(0 \leq i \leq 3)$ are created using the 1-D filters $g_0^{(1d)}$ and $g_1^{(1d)}$. It turns out that one needs to filter the rows and columns of the input signal by $g_0^{(1d)}$ and $g_1^{(1d)}$ once. Hence, the complexity of filtering by $G_i^{\mathtt{M}}(z)$, $(0 \leq i \leq 3)$ will be $2 \times (l_g - 1)/2 + 2 \times (l_g + 1)/2 = 2l_g$ MPS and $2l_g - 4$ APS. Consequently, the overall complexity is $2(l_g + l_h)$ MPS

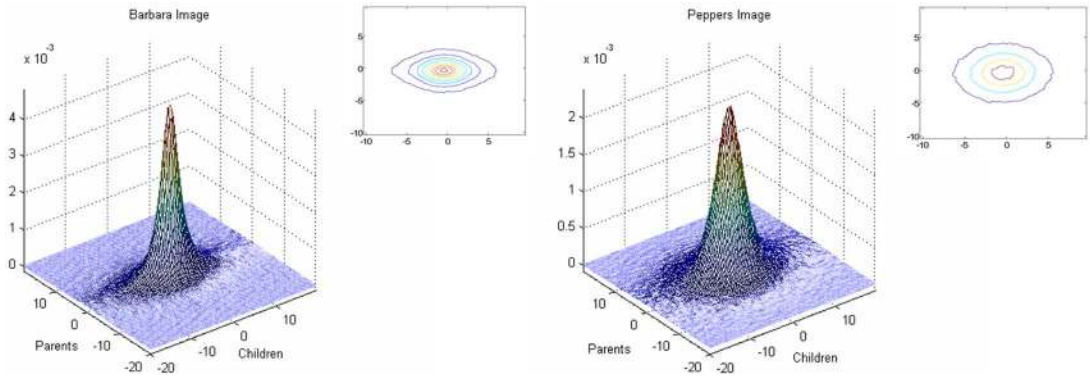

Fig. 10. Normalized joint histograms along with their contour plots of parents children of the STICT coefficients for the images *Barbara* and *Peppers*. (Color version available online at http://ieeexplore.ieee.org.)

TABLE I
PSNR VALUES OF THE DENOISING EXPERIMENTS

Image	σ	Noisy Image	Adaptive Wiener	WT (HT)	CT (HT)	TIWT (HT)	DTCWT (HT)	STICT (HT)	TICT (HT)	TIWT (BS)	DTCWT (BS) [32]	BLS-GSM [29]	STICT (BS)
Barbara	5	34.15	29.12	33.75	33.64	36.54	36.04	*36.75*	**37.07**	37.85	37.09	**37.96**	*37.95*
	10	28.13	28.31	29.86	30.17	32.58	32.66	*33.19*	**33.49**	33.72	33.50	*34.40*	**34.42**
	20	22.15	26.44	25.80	26.49	28.26	28.93	*29.26*	**29.53**	29.41	29.78	**30.60**	*30.59*
	40	16.38	23.65	22.44	23.17	24.53	25.02	*25.42*	**25.70**	25.33	26.35	*26.70*	**26.77**
	70	12.25	21.03	20.51	21.04	22.19	22.28	*22.54*	**22.78**	22.38	23.44	*23.54*	**23.57**
	100	10.16	19.41	19.41	19.76	20.60	20.62	*20.75*	**20.95**	20.67	*21.41*	**21.51**	21.40
Boats	5	34.15	31.37	34.39	33.97	*36.88*	36.37	36.78	**37.11**	*38.13*	37.55	**38.17**	38.04
	10	28.14	30.44	30.76	30.59	*33.32*	33.24	33.31	**33.59**	34.19	34.02	**34.69**	*34.35*
	20	22.18	28.36	27.21	27.27	29.75	*29.80*	29.79	**30.03**	30.32	30.63	**31.14**	*30.73*
	40	16.42	25.09	23.83	24.08	*26.32*	26.20	26.25	**26.49**	26.47	*27.36*	**27.65**	27.15
	70	12.31	21.86	21.25	21.50	*23.27*	23.10	23.10	**23.33**	23.27	*24.33*	**24.41**	23.91
	100	10.20	19.84	19.73	19.83	*21.06*	21.00	20.89	**21.08**	21.12	*21.88*	**21.94**	21.55
Lena	5	34.15	34.01	35.26	35.00	37.33	*37.35*	37.30	**37.52**	**38.27**	38.00	*38.22*	38.20
	10	28.13	32.66	32.10	32.10	34.53	*34.71*	34.67	**34.89**	35.08	35.30	**35.60**	*35.44*
	20	22.13	30.00	28.58	28.91	31.35	31.45	*31.52*	**31.75**	31.54	*32.35*	**32.63**	32.30
	40	16.35	26.10	24.97	25.62	27.83	27.67	*27.94*	**28.22**	27.68	*29.24*	**29.39**	28.82
	70	12.22	22.52	22.20	22.78	*24.55*	24.31	24.52	**24.82**	24.23	*25.93*	**25.96**	25.35
	100	10.15	20.46	20.64	21.98	*22.20*	22.09	22.15	**22.39**	22.05	*23.22*	**23.30**	22.79
Peppers	5	34.21	34.21	34.24	33.75	*35.86*	**36.04**	35.68	35.83	**36.88**	*36.52*	36.46	36.46
	10	28.25	32.87	31.83	31.53	33.91	*33.99*	33.82	**34.00**	*34.49*	34.27	**34.57**	34.43
	20	22.32	30.09	28.49	28.50	*30.97*	30.91	30.92	**31.15**	31.12	31.49	**31.92**	*31.60*
	40	16.59	25.79	24.47	24.82	*27.06*	26.79	26.99	**27.26**	26.78	*28.00*	**28.21**	27.77
	70	12.46	21.84	21.12	21.62	*23.29*	23.00	23.20	**23.45**	22.90	**24.29**	*24.26*	23.91
	100	10.30	19.55	19.28	19.58	*20.70*	20.58	20.61	**20.80**	20.54	**21.48**	*21.44*	21.19

and $2(l_g + l_h - 1)$ APS. For an L-level TILP, the complexity will be L times the complexity of a single-level TILP.

3) DFB: Although the quincunx sampling matrix is nonseparable and thus filtering using fan filters is nonseparable, Phoong *et al.* [28] proposed an efficient approach, which provides separable filtering in the polyphase domain. Suppose that the kernel function $\beta(z)$ in the ladder network [28] has length l_β, which generates the 2-D synthesis filters with support sizes of $(2l_\beta-1, 2l_\beta-1)$ and $(4l_\beta-3, 4l_\beta-3)$. Then, the complexity of the *quincunx filter bank* (QFB) is $2l_\beta$ MPS and $2l_\beta - 1$ APS. Since we iterate the QFB at all channels for the higher directional levels, the complexity of the $\hat{l}$-level DFB will be $\hat{l}$ times and that of a modified DFB is $(\hat{l}+1)/2$ times the complexity of the QFB.

4) TIDFB: In this case, opposite to the DFB, we have to perform nonseparable filtering at some levels due to omitting the subsampling operations. Nevertheless, we show that we can have a complexity similar to the separable filtering. Using again the filters designed in [28], we have the synthesis filters for QFB as follows:

$$H_0(z_1, z_2) = \left(\frac{1}{2}\right)\left(z_1^{-2l_\beta} + z_1^{-1}\beta(z_1 z_2^{-1})\beta(z_1 z_2)\right)$$

and $H_1(z_1, z_2) = z_1^{-4l_\beta+1} - \beta\left(z_1 z_2^{-1}\right)\beta(z_1 z_2)H_0(z_1, z_2)$

provided that the sampling matrix is $Q = \begin{bmatrix} 1 & 1 \\ 1 & -1 \end{bmatrix}$.

Here, since both $\beta\left(z_1 z_2^{-1}\right)$ and $\beta(z_1 z_2)$ are diagonal matrices having l_β nonzero elements, the complexity of the QFB is

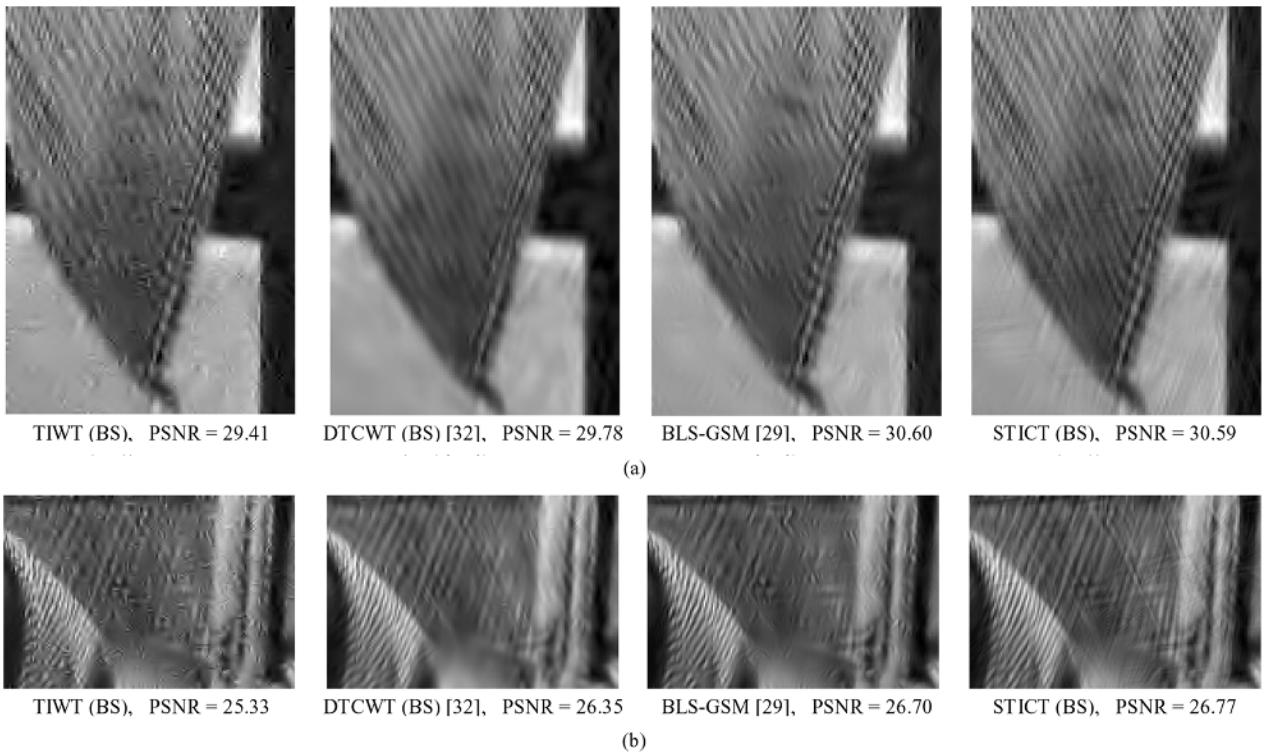

Fig. 11. Denoising results of the *Barbara* image when (a) $\sigma = 20$ and (b) $\sigma = 40$.

$4l_\beta$ MPS and $4l_\beta - 2$ APS, which is the same as the separable case. In the second level of the TIDFB, we upsample the filters by Q, where $\beta\left(z_1 z_2^{-1}\right)\beta(z_1 z_2)$ transforms to $\beta\left(z_2^2\right)\beta\left(z_1^2\right)$ and therefore, for *each QFB* we reach the same complexity as the first level. For higher levels, in addition to the sampling matrix Q, we have resampling matrices, as well. The overall sampling matrices for these levels after the second level are in the form of [26]

$$\begin{bmatrix} 2^{\hat{l}-2} & 0 \\ 0 & 1 \end{bmatrix} \text{ or } \begin{bmatrix} 1 & 0 \\ 0 & 2^{\hat{l}-2} \end{bmatrix}.$$

Consequently, for a level $\hat{l} \geq 3$, $\beta\left(z_2^2\right)\beta\left(z_1^2\right)$ converts to $\beta\left(z_2^2\right)\beta\left(z_1^{2^{\hat{l}-1}}\right)$ or $\beta\left(z_2^{2^{\hat{l}-1}}\right)\beta\left(z_1^2\right)$, which indicates that for each QFB at these levels also we have the same complexity as the first level. Since the total number of the QFBs employed in an $\hat{l}$-level TIDFB is $2^{\hat{l}} - 1$ and that of the modified TIDFB is $2^{\hat{l}-1}$, $(\hat{l} \geq 2)$, the complexity of these schemes will be $4l_\beta(2^{\hat{l}} - 1)$ MPS and $(4l_\beta - 2)(2^{\hat{l}} - 1)$ APS, and $4l_\beta 2^{\hat{l}-1}$ MPS and $(4l_\beta - 2)2^{\hat{l}-1}$ APS, respectively.

5) STICT: In this case, for an L-level STICT employing (modified) DFBs with $\hat{l}_i$, $(1 \leq i \leq L)$ levels, we have $2L(l_h + l_g) + 6l_\beta \sum_{i=1}^{L} \hat{l}_i + 2l_\beta L$ MPS and $2L(l_h + l_g - 1) + 3(2l_\beta - 1)\sum_{i=1}^{L} \hat{l}_i + (2l_\beta - 1)L$ APS.

6) TICT: Considering the complexity of the TILP and (modified) TIDFB, an L-level TICT having TIDFBs with $\hat{l}_i$, $(1 \leq i \leq L)$ levels has the complexity of $2L(l_h + l_g) + 12l_\beta \sum_{i=1}^{L} 2^{\hat{l}_i} - 8l_\beta L$ MPS and $2L(l_h + l_g - 1) + (4l_\beta - 2)\sum_{i=1}^{L}\left(3\left(2^{\hat{l}_i}\right) - 2\right)$ APS.

Note that, in the above calculations, we have considered general forms of the filters. If, however, linear-phase filters are employed, we can use about half of the filter lengths in the above complexities. We see that due to the (modified) TIDFB, both the complexity and redundancy ratio of the TICT are exponentially proportional to the directional levels $\hat{l}_i$, $(1 \leq i \leq L)$, whereas they appear as linear terms in those of the STICT. Hence, significant reductions in complexity can be achieved when using STICT, especially when using a high number of levels.

IV. Image Denoising

One of the major applications of the wavelet transform is denoising. For images, however, directionality is an important feature that the regular WT lacks. It follows that, when one denoises images using wavelets, the edges and fine details are smeared. Therefore, using subband decompositions having the feature of directionality as well as a good nonlinear approximation property would result in superior image denoising performance [16], [32], [35]. The CT has been shown to be a better alternative choice than the WT at some cases [13], [16], [18], [30]. In [18], a cycle-spinning algorithm is employed to improve the denoising performance of contourlets. Although it is equivalent to a TI denoising if all of the possible shifts of the input image are used [8], the computational complexity of this procedure for an image of size $N \times N$ is N^2 times that of the CT, which consequently makes this algorithm almost prohibitive for rather large-size images. Our preliminary work on contourlet TI denoising demonstrated the effectiveness of the STICT in image

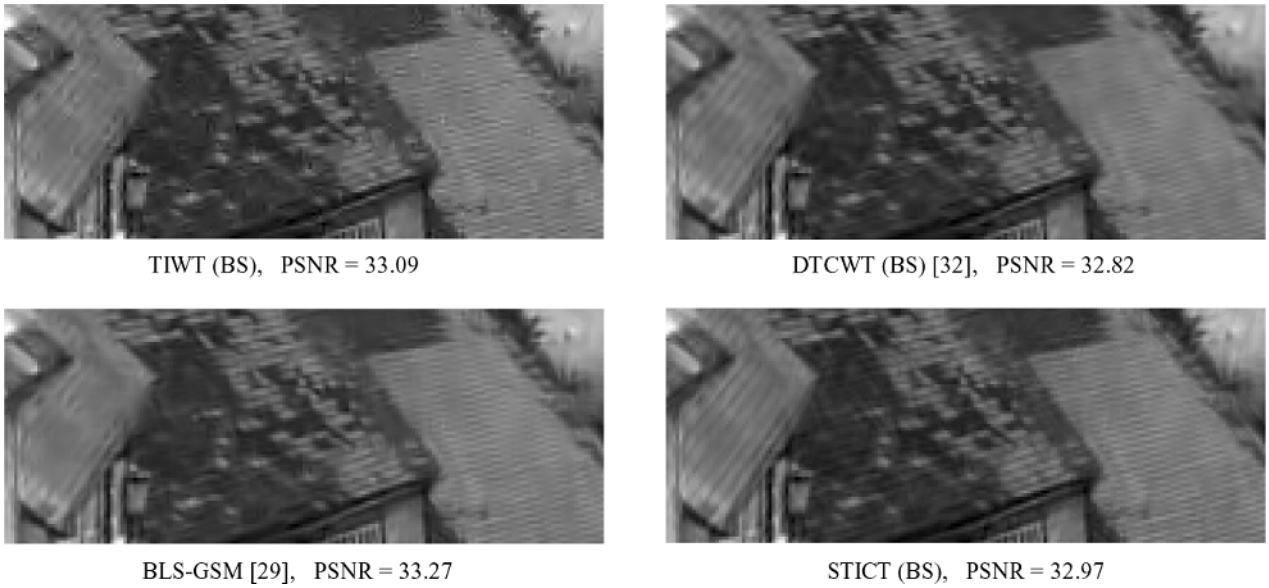

Fig. 12. Denoising results of the *GoldHill* image when $\sigma = 10$.

denoising [16]. Here, we improve our method through finding a suitable shrinkage function.

A. STICT Denoising Scheme Using Bivariate Shrinkage

One of the most crucial factors in image denoising is the method of shrinkage. Because of the interscale and intrascale dependencies amongst the transform coefficients, it is of key importance to build the shrinkage operation upon an appropriate probability model to account for these dependencies. Bivariate shrinkage is a recent shrinkage approach, which in addition to taking into account the dependencies among the coefficients in each subband, considers the parent-children relationship into the maximum *a posteriori* (MAP) probability estimation [31]. In this work, we introduce a new image denoising scheme based on the proposed STICT and incorporating bivariate shrinkage. This shrinkage approach is established through modeling the joint *probability distribution function* (PDF) of parents and children of the transform coefficients. For wavelets and also dual-tree complex wavelet coefficients, [31] proposed the following non-Gaussian joint PDF

$$p_{\mathbf{X}}(\mathbf{x}) = \frac{3}{2\pi\sigma^2} e^{(\sqrt{3}/\sigma)\sqrt{x_1^2+x_2^2}} \tag{3}$$

where x_1 and x_2 denote parents and children. The main advantage of this model is that it provides a closed-form shrinkage function that results in easy realization and also generates competitive results in comparison with the more sophisticated models [31].

For the STICT, we need to first study the joint PDF of parents-children. In this case, we propose a parent-children relationship, which is similar to the one introduced for the CT coefficients [30]. Suppose that we have the STICT with $\hat{l}_i$, $(1 \leq i \leq L)$ directional levels, then we consider the following parent-children relationship, where $\tilde{m} = (m_1/2, m_2)^T$ for horizontal and $\tilde{m} = (m_1, m_2/2)^T$ for vertical subbands (see the equation shown at the bottom of the page). For subbands corresponding to y_0 or y_1 (see Fig. 7), the children lie at the same position where the parents are in the next coarser level. Note that for the approximation subband $\eta_L(m)$, all the directional subbands at the previous level are children subbands with a similar relationship that was mentioned above. Using this definition, in Fig. 10, we demonstrate the normalized joint histogram of parents-children for the *Barbara* and *Peppers* images, when an STICT with $\{\hat{l}_i\}_{1\leq i\leq 2} = \{3,3\}$ directional levels is employed. We see that the joint histograms are similar to that of the wavelet coefficients (see [31]) and, hence, we propose to use the model (3) with local variance estimation for our bivariate shrinkage function in the STICT domain.

B. Simulation and Results

To evaluate the proposed schemes, we performed several experiments on a variety of images all of size 512 × 512. Here, we also provide the WT, CT, and TICT denoising results using hard thresholding. For the sake of comparison, we also employed some of the state-of-the-art methods in the literature such as the *dual-tree complex wavelet transform* (DTCWT)

parent child(ren)

$$\eta^{(\mathtt{d})}_{\mathtt{i},\mathtt{k}}(m) \rightarrow \begin{cases} \eta^{(\mathtt{d})}_{\mathtt{i}+1,\mathtt{k}}(m), & \text{if } \hat{l}_{\mathtt{i}+1} = \hat{l}_{\mathtt{i}},\ (\mathtt{i} \neq L) \\ \eta^{(2\mathtt{d}-1)}_{\mathtt{i}+1,\mathtt{k}}(\tilde{m}) \text{ and } \eta^{(2\mathtt{d})}_{\mathtt{i}+1,\mathtt{k}}(\tilde{m}), & \text{if } \hat{l}_{\mathtt{i}+1} = \hat{l}_{\mathtt{i}} + 1,\ (\mathtt{i} \neq L) \end{cases}$$

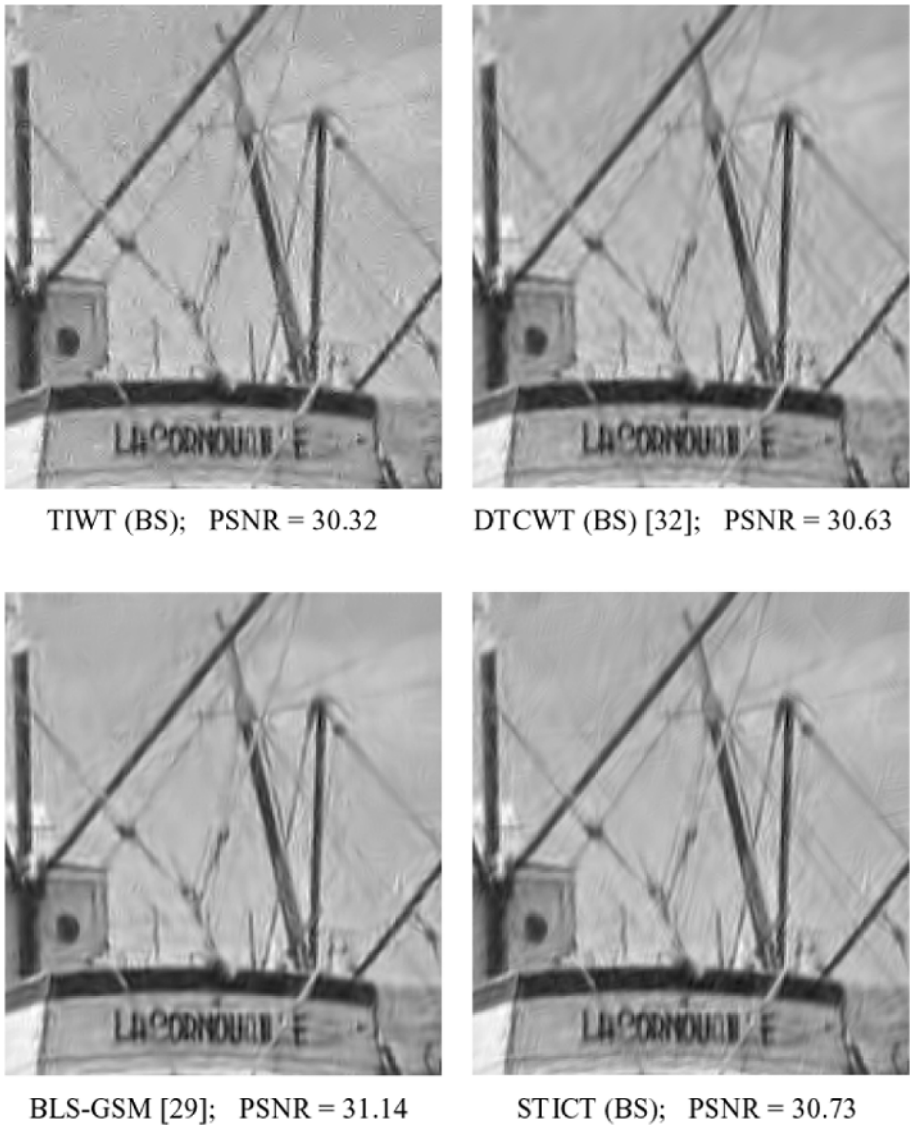

Fig. 13. Denoising results of the *Boats* image when $\sigma = 20$.

with both *hard thresholding* (HT) and *bivariate shrinkage* (BS) [32], and the BLS-GSM denoising method proposed by Portilla *et al.* [29] (using full steerable pyramid with window size (3,3) and inclusion of parents). Furthermore, we used a *TI* (or undecimated) *wavelet transform* (TIWT) as well as adaptive wiener filter (function *wiener2* in Matlab) using a window size of (5,5). Note that using the *generalized algorithme à trous* proposed in Section II, we can easily construct the TIWT. Hence, a TIWT with L levels has a redundancy factor of $3L+1$ and complexity of $2L(l_g+l_h)$ MPS and $2L(l_g+l_h-2)$ APS, where l_h and l_g are the lengths of the 1-D analysis filters $h^{(1d)}$ and $g^{(1d)}$.

The filters we used for the TIWT and TILP in the (S)TICT are biorthogonal Daubechies 9/7. Further, we used five levels for the TIWT and a four-level TILP in the (S)TICT. For the (modified) DFB and TIDFB, we utilized the fan filters designed in [28] with $l_\beta = 12$ and, hence, support sizes of (23,23) and (45,45). We applied $\{\hat{l}_i\}_{1\le i\le 4} = \{3,3,2,2\}$ directional levels to the (S)TICT except for the STICT (BS) for the *Barbara* image where we used $\{\hat{l}_i\}_{1\le i\le 4} = \{4,3,3,2\}$. Note that if we use more directions and levels in the (S)TICT, there will be more artifacts introduced in the denoised images.

The images were contaminated by a zero-mean Gaussian white noise with a standard deviation of σ. For all the denoising schemes, we assumed that σ is unknown and we estimated it using the robust median estimator [15]. Moreover, we mirror-extended the noisy images to avoid boundary distortion. Although the size of the noisy images is rather large, the PSNR values of the denoising results change slightly (usually up to ± 0.1 dB) when we use a different noise instance. Hence, to obtain more accurate PSNR values, we repeated each denoising experiment ten times using different noise realizations and found the average of PSNR values. We also clipped the noisy images to set the pixel values in the allowable range of 0 to 255.

Table I shows the PSNR values of the denoising results when the standard deviation of the input noise is varying between $\sigma = 5$ and $\sigma = 100$. In the first part of the table, we used hard thresholding to compare different transforms for denoising. We also included adaptive wiener filter results in this part. As seen, our proposed TICT (HT) method outperforms the other methods

in most cases. In addition, the STICT (HT) provides competitive PSNR values to the other leading schemes.

The second part of Table I shows our proposed STICT (BS) denoising results as well as those of the TIWT (BS), DTCWT (BS) [32], and BLS-GSM [29]. The computational times for these methods on the computer we ran the simulation were roughly 35, 17, 5, and 95s, respectively. As seen in Table I, for low and moderate noise ($\sigma \leq 20$), our method performs competitively to other methods but for higher power of noise this approach slightly degrades due to the amount of introduced artifacts.

Visually, however, the proposed STICT (BS) method performs better in recovering very fine details found in some images such as the *Barbara* image. Fig. 11 shows the visual results of the *Barbara* image where the superior performance of the proposed approach is clear. Another visual example is depicted in Fig. 12, which illustrates part of the *GoldHill* image. Again, we can see that the details over the roofs are better recovered using the STICT (BS) approach. Finally, Fig. 13 depicts another example from the *Boats* image. Here, we can compare the artifacts introduced around edges by these methods. Note that both the TIWT and dual-tree complex wavelets produce more (visible) artifacts around strong edges. The proposed method provides similar performance to that of the BLS-GSM in this figure.

V. Conclusion

In this work, we studied and developed new approaches for converting a general multichannel multidimensional subsampled FB to a translation-invariant or nonsubsampled FB. Particularly, we extended the *algorithme à trous*, which has been introduced for 1-D wavelets, to a *generalized algorithme à trous*, which is applicable to a general multidimensional and multichannel FB framework. Using the proposed *generalized algorithme à trous*, as well as incorporating modified versions of the DFB, we constructed the new scheme of the TICT. We also proposed STICT to reduce the high redundancy and complexity of the TICT. Then, we used a competent Bayesian-based shrinkage approach in conjunction with the proposed STICT to create an efficient denoising scheme. Our results indicate the potential of this new scheme in image denoising.

Acknowledgment

The authors would like to thank the reviewers for their helpful comments, which led to a significant improvement in the paper.

References

[1] J. P. Antoine, P. Carrette, R. Murenzi, and B. Piette, "Image analysis with two-dimensional continuous wavelet transform," *Signal Process.*, vol. 31, pp. 241–272, 1993.

[2] R. H. Bamberger and M. J. T. Smith, "A filter bank for the directional decomposition of images: Theory and design," *IEEE Trans. Signal Process.*, vol. 40, no. 4, pp. 882–893, Apr. 1992.

[3] G. Beylkin, "On the representation of operators in bases of compactly supported wavelets," *SIAM J. Numer. Anal.*, vol. 29, pp. 1716–1740, 1992.

[4] P. J. Burt and E. H. Adelson, "The Laplacian pyramid as a compact image code," *IEEE Trans. Commun.*, vol. 31, no. 4, pp. 532–540, Apr. 1983.

[5] E. J. Candes and D. L. Donoho, "Curvelets—A surprisingly effective nonadaptive representation for objects with edges," in *Curve and Surface Fitting*. Nashville, TN: Vanderbuilt Univ. Press, 1999.

[6] ——, "Ridgelets: A key to higher-dimensional intermittency?," *Phil. Trans. Roy. Soc. Lond. A.*, pp. 2495–2509, 1999.

[7] I. Cohen, S. Raz, and D. Malah, "Orthonormal shift-invariant wavelet packet decomposition and representation," *Signal Process.*, vol. 57, no. 3, pp. 251–270, Mar. 1997.

[8] R. R. Coifman and D. L. Donoho, "Translation invariant de-noising," in *Wavelets and Statistics*. New York: Springer-Verlag, 1995, vol. 103, Springer Lecture Notes in Statistics, pp. 125–150.

[9] Z. Cvetkovic and M. Vetterli, "Oversampled filter banks," *IEEE Trans. Signal Process.*, vol. 46, no. 5, pp. 1245–1255, May 1998.

[10] I. Daubechies, *Ten Lectures on Wavelets*. Philadelphia, PA: SIAM, 1992.

[11] M. N. Do and M. Vetterli, "Directional Multiresolution Image Representations," Ph.D. dissertation, EPFL, Lausanne, Switzerland, 2001.

[12] M. N. Do and M. Vetterli, "Contourlets," in *Beyond Wavelets*, G. V. Welland, Ed. New York: Academic, 2003, pp. 1–27.

[13] ——, "The contourlet transform: An efficient directional multiresolution image representation," *IEEE Trans. Image Process.*, vol. 14, no. 12, pp. 2091–2106, Dec. 2005.

[14] ——, "Framing pyramids," *IEEE Trans. Signal Process.*, vol. 51, no. 9, pp. 2329–2342, Sep. 2003.

[15] D. L. Donoho and I. M. Johnstone, "Ideal spatial adaptation by wavelet shrinkage," *Biometrika*, vol. 81, no. 3, pp. 425–455, 1994.

[16] R. Eslami and H. Radha, "Image denoising using translation-invariant contourlet transform," in *Proc. IEEE Int. Conf. Acoustics, Speech, and Signal Processing*, Mar. 2005, vol. 4, pp. 557–560.

[17] R. Eslami and H. Radha, "New image transforms using hybrid wavelets and directional filter banks: Analysis and design," in *Proc. IEEE Int. Conf. Image Processing*, Genova, Italy, Sep. 2005, pp. 733–736.

[18] ——, "The contourlet transform for image de-noising using cycle spinning," in *Proc. Asilomar Conf. Signals, Systems, and Computers*, Pacific Grove, CA, Nov. 2003, pp. 1982–1986.

[19] M. Holschneider, R. Kronland-Martinet, J. Morlet, and P. Tchamitchian, "A real-time algorithm for signal analysis with the help of the wavelet transform," in *Wavelets, Time-Frequency Methods and Phase Space*. Berlin, Germany: Springer-Verlag, 1989, pp. 289–297.

[20] N. G. Kingsbury, "Complex wavelets for shift invariant analysis and filtering of signals," *Appl. Comput. Harmon. Anal.*, vol. 10, no. 3, pp. 234–253, May 2002.

[21] ——, "Image processing with complex wavelets," *Phil. Trans. Roy. Soc. Lond.*, Sep. 1999.

[22] S. Mallat, *A Wavelet Tour of Singnal Processing*, 2nd ed. New York: Academic, 1998.

[23] S. Mallat and S. Zhong, "Characterization of signals from multiscale edges," *IEEE Trans. Pattern Anal. Mach. Intell.*, vol. 14, no. 7, pp. 710–732, Jul. 1992.

[24] F. G. Meyer and R. R. Coifman, "Brushlets: A tool for directional image analysis and image compression," *Appl. Comput. Harmon. Anal.*, vol. 4, pp. 147–187, 1997.

[25] G. P. Nason and B. W. Silverman, "The stationary wavelet transform and some statistical applications," in *Wavelets and Statistics*. New York: Springer-Verlag, 1995, vol. 103, Springer Lecture Notes in Statistics, pp. 281–299.

[26] S. Park, M. J. T. Smith, and R. M. Mersereau, "Improved structures of maximally decimated directional filter banks for spatial image analysis," *IEEE Trans. Image Process.*, vol. 13, no. 11, pp. 1424–1431, Nov. 2004.

[27] J.-C. Pesquet, H. Krim, and H. Carfantan, "Time-invariant orthonormal wavelet representations," *IEEE Trans. Signal Process.*, vol. 44, no. 8, pp. 1964–1970, Aug. 1996.

[28] S. M. Phoong, C. W. Kim, P. P. Vaidyanathan, and R. Ansari, "A new class of two-channel biorthogonal filter banks and wavelet bases," *IEEE Trans. Signal Process.*, vol. 43, no. 3, pp. 649–665, Mar. 1995.

[29] J. Portilla, V. Strela, M. J. Wainwright, and E. P. Simoncelli, "Image denoising using scale mixtures of gaussians in the wavelet domain," *IEEE Trans. Image Process.*, vol. 12, no. 11, pp. 1338–1351, Nov. 2003.

[30] D. D.-Y. Po and M. N. Do, "Directional multiscale modeling of images using the contourlet transform," *IEEE Trans. Image Process.*, vol. 15, no. 6, pp. 1610–1620, Jun. 2006.

[31] L. Sendur and I. W. Selesnick, "Bivariate shrinkage functions for wavelet-based denoising exploiting interscale dependency," *IEEE Trans. Signal Process.*, vol. 50, no. 11, pp. 2744–2756, Nov. 2002.

[32] ——, "Bivariate shrinkage with local variance estimation," *IEEE Signal Process. Lett.*, vol. 9, no. 12, pp. 438–441, Dec. 2002.
[33] M. J. Shensa, "The discrete wavelet transform: Wedding the à trous and Mallat algorithms," *IEEE Trans. Signal Process.*, vol. 40, no. 10, pp. 2464–2482, Oct. 1992.
[34] E. P. Simoncelli, W. T. Freeman, E. H. Adelson, and D. J. Heeger, "Shiftable multi-scale transforms," *IEEE Trans. Inf. Theory*, vol. 38, no. 2, pp. 587–607, Mar. 1992.
[35] J.-L. Starck, E. J. Candes, and D. L. Donoho, "The curvelet transform for image denoising," *IEEE Trans. Image Process.*, vol. 11, no. 6, pp. 670–684, Jun. 2002.
[36] P. P. Vaidyanathan, *Multirate Systems and Filter Banks*. Englewood Cliffs, NJ: Prentice-Hall, 1993.
[37] M. Vetterli and J. Kovacevic, *Wavelets and Subband Coding*. Englewood Cliffs, NJ: Prentice-Hall, 1995.
[38] R. Zuidwijk, "Continuous and discrete wavelet X-ray transform," *SPIE Wavelet Application in Signal and Image Processing V*, pp. 357–366, 1997.

Ramin Eslami (S'02–M'06) received the B.S. degree in electrical engineering from Iran University of Science and Technology, Tehran, Iran, in 1994, the M.S. degree in biomedical engineering from Sharif University of Technology, Tehran, Iran, in 1997, and the Ph.D. degree in electrical engineering from Michigan State University (MSU), East Lansing.

Currently, he is a Postdoctoral Fellow in the Department of Electrical and Computer Engineering, McMaster University, Hamilton, ON, Canada. From 2002 to 2006, he was a Research Assistant in the Department of Electrical and Computer Engineering, MSU. He was an Instructor in the Electrical Engineering Department, Aeronautical University of Shahid Sattari, Tehran, Iran, from 1998 to 2000. His research interests include image and multidimensional signal processing, wavelets and filter banks, coding, denoising, and watermarking.

Hayder Radha received the B.S. degree (with honors) from Michigan State University (MSU), East Lansing, in 1984, the M.S. degree from Purdue University, West Lafayette, IN, in 1986, and the Ph.M. and Ph.D. degrees from Columbia University, New York, in 1991 and 1993, respectively, all in electrical engineering.

He is a Professor of Electrical and Computer Engineering at MSU. He joined MSU in 2000 as an Associate Professor in the Department of Electrical and Computer Engineering. Between 1996 and 2000,he was with Philips Research, where he worked as a Principal Member of Research Staff and then as a Consulting Scientist in the Video Communications Research Department. At Philips Research, he initiated the Internet Video Project and led a team of researchers working on scalable video coding, networking and streaming algorithms. He became a Philips Research Fellow in 2000. Prior to working at Philips Research, he was with Bell Labs where he worked between 1986 and 1996 in the areas of digital communications, signal/image processing, and broadband multimedia. He served as Co-Chair and Editor of the ATM and LAN Video Coding Experts Group of the ITU-T from 1994 to 1996. His research interests include coding and communications, multimedia networking, stochastic modeling, and image and video processing and compression, and he has authored more than 100 peer-reviewed papers and holds 24 U.S. patents in these areas.

Dr. Radha is a recipient of the Bell Labs Distinguished Member of Technical Staff Award, the AT&T Bell Labs Ambassador Award, AT&T Circle of Excellence Award, the Withrow Distinguished Scholar Award for outstanding contributions to engineering, and the Microsoft Research Content and Curriculum Award.